Chapter 1

The Flat Plate at Shallow Incidence

1.1 Introduction

This chapter investigates ability of turbulence models to reproduce the ‡ow over ‡at plates at shallow angles of incidence. This case poses signi…cant relevance to sail ‡ows due to the formation of a separation bubble at the leading edge of the type that regularly appears in sail ‡ows. Such bubbles are always present for downwind sails and are common for genoas with thin headfoils. This type of leading edge bubble may also be present for various thin airfoils such as those often used for turbine blades. Validation will be carried out through comparison to wind tunnel results compiled by Crompton [1] and particular attention will be paid to the structure of the leading edge bubble and the recovery of the turbulent boundary layer after reattachment.

1.1.1 Flow structure

The general structure of the ‡ow past a ‡at plate at incidence is illustrated in Figure 1.1. At zero incidence the forward stagnation point rests on the tip of the leading edge, the plate divides the ‡ow cleanly and laminar boundary layers develop immediately on either side of the plate. As the angle of attack is increased the stagnation point moves to the pressure side of the plate and ‡uid is forced back around the leading edge due to the pressure di¤erence that exists across the tip. If the leading edge is sharp then the ‡ow is forced to detach at the leading edge. Immediately after separation a shear layer forms that rapidly undergoes transition into a turbulent shear layer provided the Reynolds number is not unrealistically small (for creeping ‡ows the ‡ow may not separate). This shear layer curves back towards the plate due to its high entrainment rate (causing the layer to thicken) and suction on the upper surface near the leading edge. For shallow angles of incidence (typically $< 7^{\pm}$) the shear layer reattaches some distance, X_R, downstream of the leading edge. At the reattachment point the shear layer bifurcates and a portion of the ‡ow is directed upstream to form the recirculation region. The remainder (which is the majority) of the ‡uid in the shear layer progresses downstream and gradually develops into a turbulent boundary layer. This region downstream of the reattachment point is known as the recovery region where the boundary layer attempts to recover to a state of turbulent equillibrium. This region is of particular signi…cance to sail ‡ows since the structure of the boundary layer during recovery dictates not only the local pressure coe¢cient but also the size and structure of any trailing edge separation regions that may form downstream. Consquently the nature of the boundary layer after reattachment can have

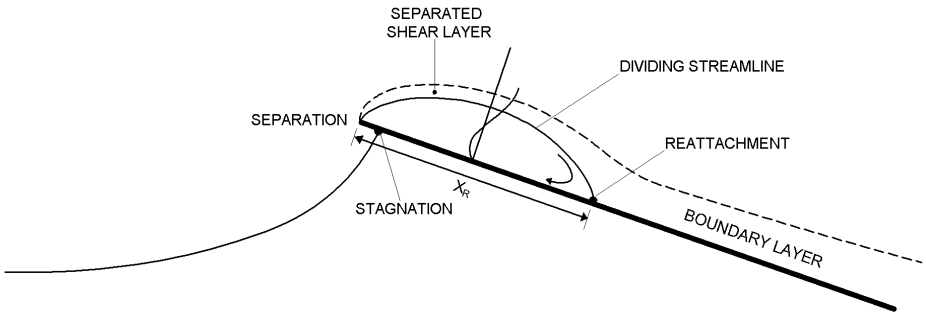

Figure 1.1: Schematic of the ‡ow past a ‡at plate at shallow incidence.

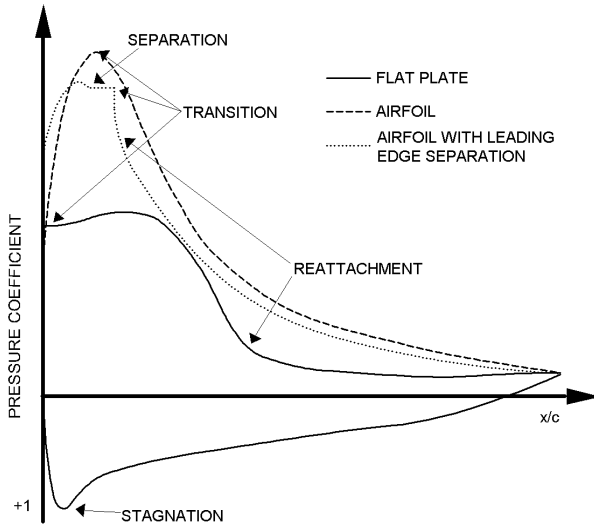

Figure 1.2: Typical pressure coe¢cient plots.

a signi…cant impact on the lift coe¢cient.

A typical pressure coe¢cient distribution for a ‡at plate at shallow incidence is illustrated in Figure 1.2. Also presented are typical pressure coe¢cient plots for a generic airfoil and an airfoil with a leading edge separation bubble. The ‡at plate experiences a signi…cantly smaller suction peak at the leading edge compared with the airfoils due to its inability to sustain any attached ‡ow in this region. Reattachment occurs approximately at the conclusion of the adverse pressure gradient that exists over the aft half of the bubble.

1.1.2 The thin airfoil bubble

The separation bubble that forms due to the inability of the boundary layer to remain attached around the sharp leading edge is known as the “thin airfoil bubble”. The shear layer that develops in the thin airfoil bubble is immediately unstable and turbulent transition occurs rapidly after separation at the leading edge. Crompton [1] reported that in all cases transition occurred upstream of $x/c = 0.025$ and that intermittency was observed well upstream of this point. Consequently it is hypothesised that eddy

viscosity models (which e¤ectively predict instantaneous transition to turbulence) can be applied much more suitably to the thin airfoil bubble than to ‡ows that involve regions of laminar ‡ow.

Newman and Tse [2] found that above a Reynolds number of $2{:}5 \pounds 10^5$ the reattachment length was insensitive to changes in Reynolds number. Crompton [1] found Reynolds number insensitivity of the reattchment length above a Reynolds number of approximately 10^5. This limit increased slightly as the incidence reduced due to greater viscous e¤ects in the shallower separation bubbles. The reattachment length is primarily dependent on the rate of turbulent entrainment in the shear layer. At low Reynolds numbers as the Reynolds number is increased so does the entrainment rate and hence the reattachment length shortens. As the Reynolds number is increased further the maximum entrainment rate is reached as shear layer enters a state of turbulent equllibrium. At this point the reattachment length begins to lengthen again due to a reduction of shear layer thickness associated with increasing Reynolds number (due to lower di¤usive e¤ects resulting in lower shear layer spreading rates). At approximately 10^5 this thickness reduction becomes negligible and the shear layer pro…le (and hence also the reattachment length) becomes independent of Reynolds number.

Crompton's results also show that between a Reynolds number of $0{:}53 \pounds 10^5$ and $2{:}13 \pounds 10^5$ the transition point is independent of Reynolds number and …xed at approximately $2 ¡ 2{:}5\%c$. This implies that the mechanism initiating transition is not driven by the freestream ‡ow (since this is signi…cantly dependent on Reynolds number) but instead transition occurs very close to the leading edge due to a process called shear layer ‡apping [3] where alternate vortices are shed from the origin of the shear layer. Crompton [1] detected low frequency unsteadyness at too large a scale to be associated with the large eddies and concluded that vortical structures, of the type associated with shear layer ‡apping, must be present.

Since the reattachment process is always a turbulent one, the downstream recovery of the turbulent boundary layer can be expected to be only weakly dependent of Reynolds number. However the within the separation bubble Reynolds number dependence can be expected. As the shear layer bends towards the surface the normal velocity ‡uctuations are damped by the impending wall. Also as the shear layer bifurcates at the reattachment point the large eddies are split into pairs of smaller eddies. These two e¤ects contribute to a drop in turbulent shear stress around the reattachment point. The reversing ‡uid is subject to a strong favourable pressure gradient and subsequently it accelerates and reaches a maximum velocity of approximately $0{:}4U_1$ at approximately half way along the length of the bubble. This favourable pressure gradient also has a stabilising e¤ect on the reverse ‡ow boundary layer and a signi…cant drop in turbulence intensity was recorded over this region [1]. Corresponding to this drop in turbulence intensity the velocity gradients near the surface reduce and become more laminar-like, the favourable pressure gradient is initiating relaminarisation. Near the front of the separation bubble the pressure gradient is adverse to the reversing ‡ow and the laminar-like boundary layer is prone to separate. Consequently a small secondary separation bubble develops near the leading edge. The length of this separation bubble varies with both angle of incidence and Reynolds number. The Reynolds number dependence is caused by the relaminarisation process in the reversed ‡ow boundary layer which itself is dependent on the local velocity and hence also the freestream Reynolds number.

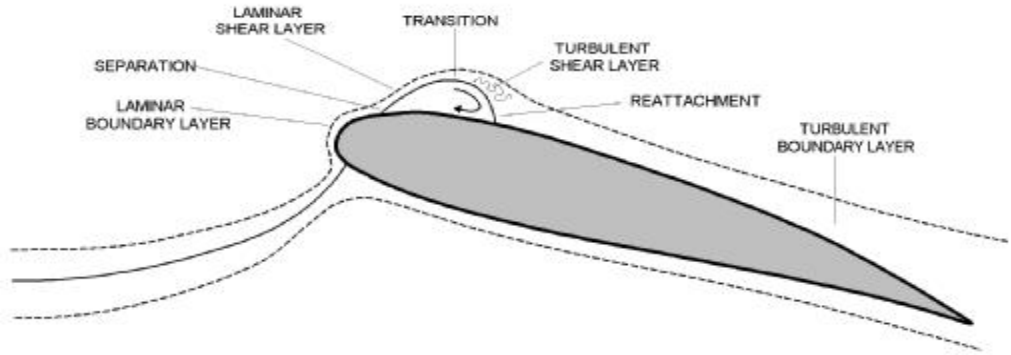

Figure 1.3: The short airfoil bubble (not to scale).

1.1.3 The short bubble

Airfoils with rounded leading edges may also exhibit separation near the leading edge (as in the airfoil case in Figure 1.2). These bubbles form due to separation of the laminar boundary layer at the onset of an adverse pressure gradient near the leading edge. Such bubbles are referred to as "short bubbles" and have been reported to have distinctly di¤erent characteristics to separation bubbles of the type illustrated in Figure 1.1 [4]. A typical short bubble is illustrated in Figure 1.3. As illustrated, transition typically occurs at the onset of the adverse pressure gradient over the rear portion of the bubble. Consequently a laminar shear layer develops that can extend across up to 60% of the bubble length. After transition the shear layer thickens rapidly and curves back towards the airfoil surface where it reattaches.

Flows involving the short separation bubble pose several di¢culties for turbulence models. The boundary layer that exists between the forward stagnation point and the separation bubble is laminar and generally turbulence models predict early transition to turbulent ‡ow in this region. As an example, for ‡at plate boundary layers under zero pressure gradient, turbulence models will predict transition to occur at a Reynolds number that is at least an order of magnitude lower than in reality [5]. Consequently for airfoil simulations involving short separation bubbles the calculated boundary layer is likely to be turbulent upstream of the separation point. Consequently the solution will exhibit an unrealistic increase in skin friction due to the high shear of turbulent boundary layers compared with laminar ones. More troublesome is the fact that a turbulent boundary layer has much steeper velocity gradients near the surface and is hence more resistant to ‡ow separation than a laminar layer. Therefore the short bubble is likely to be delayed, if not omitted entirely, in CFD simulations. Should the boundary layer in the CFD simulation remain laminar up until separation it is likely that transition will occur in the shear layer almost immediately after dettachment, upstream of the desired location. Consequently the shear layer will grow much faster which will cause the shear layer to reattach much earlier than in reality where the shear layer is laminar over the forward section of the bubble. Transition models, such as the transition version of the k ¡ $!$ model designed by Wilcox [6], have had moderate success at predicting the correct transition location for some simple ‡ows. Transition models typically use di¤erent model coe¢cients for the turbulent transport equations in the three separate regions of the ‡ow; the laminar region, transition region and the turbulent region. Tuning such a model is a di¢cult task and the position where transition occurs can be quite unpredictable between di¤erent ‡ows due to the in‡uence of the

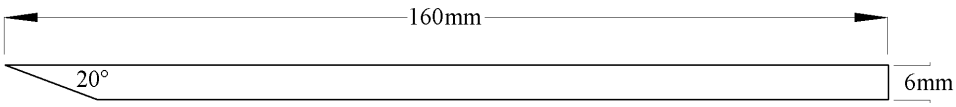

Figure 1.4: Flat plate dimensions.

local pressure gradient. In the case of the short bubble, transition actually occurs within the shear layer which poses additional di¢culties to tuning the model since the coe¢cients are usually calibrated using boundary layer ‡ows. It is also likely that within short separation bubbles some degree of relaminarisation (reverse transition) will occur because the reversed ‡ow is driven by a favourable pressure gradient. This relaminarisation process is another phenomenon that most turbulence models stuggle to predict correctly.

1.1.4 Experimental data

Of the experimental results concerned with the ‡at plate at shallow incidence the thesis by Crompton (2001), "The Thin Aerofoil Leading Edge Bubble" [1], is the most detailed. Through the use of Laser Doppler Anemometry (LDA) insight into the structure of the leading bubble was provided. Detailed LDA measurements were also taken of the developing turbulent boundary layer in the recovery region. As well as LDA measurements, surface pressures were recorded through static pressure tappings and ‡ow visualization was used to determine the reattachment lengths, X_R, of the separation bubbles.

The wind tunnel model used in the experiments has a chord length of 160*mm* and a span of 800*mm* giving an aspect ratio of 5 which was su¢cient to provide nominally two-dimensional ‡ow. In order to provide enough sti¤ness to minimise de‡ection and to facilitate the pressure tappings, the plate was constructed out of 6*mm* steel plate, giving a thickness to chord ratio of 3:75%. The leading edge of the plate was chamfered at 20 degrees in order to provide a sharp leading edge. The geometry of the leading edge can have signi…cant in‡uence on the separated shear layer. Ideally for a sharp leading edge the ‡ow will separate at any departure from zero incidence. However in reality there must be some roundedness to the leading edge which allows the boundary layer to remain attached through small departures from zero incidence.

The experiments were carried out over a range of Reynolds numbers in order to investigate the in‡uence of Reynolds number. The primary investigation was at a Reynolds number of 2:13 £ 10^5, it is at this Reynolds number that comparison between the experiments and CFD have been made.

The experimental data is provided for angles of attack, ® = 1 to 5, in 1 degree intervals. At ® = 1 the leading edge bubble is small and similar in length to chord ratio to leading edge bubbles experienced in downwind sail ‡ows. At 5 degrees the ‡ow is separated for the majority of the length of the plate and at 7 degrees the shear layer fails to reattach.

1.1.5 The CFX model

Crompton's ‡ate plate was modelled with thickness using the geometry described in Figure 1.4. The thickness and asymmetry of the plate in‡uences the ‡ow to a degree where it is necessary to use the true geometry, rather than an in…nitely thin plate for which grid generation would be simpler. The asymmetry of the plate creates a lift force even at zero degrees of incidence and which causes the ‡ow

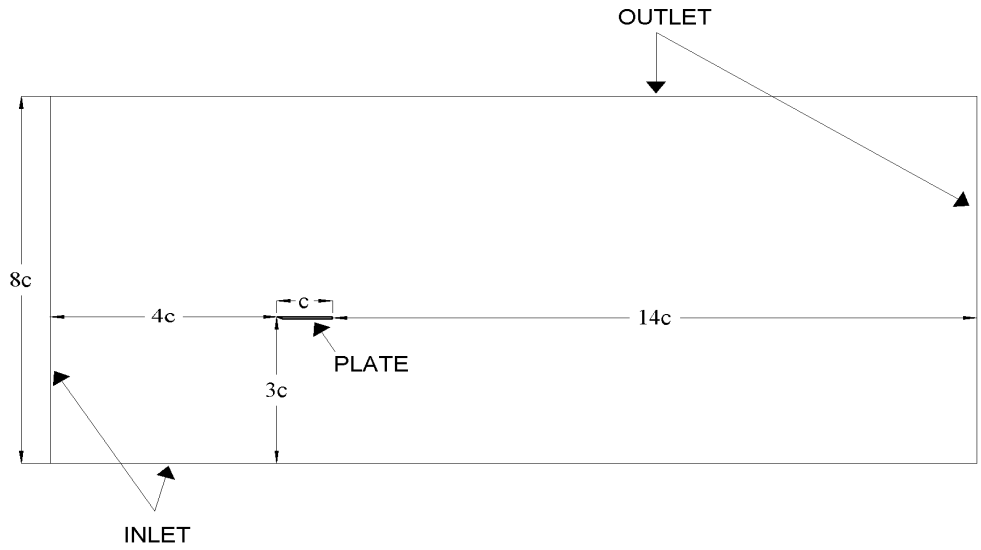

Figure 1.5: Details of the domain for the ‡at plate.

to curve upwards (in the direction of the lift axis) near the leading edge of the plate and consequently a small leading edge separation bubble forms at zero degrees. The so-called 'ideal' angle of incidence, where laminar boundary layers are able to develop on both surfaces without leading edge separation, is likely to occur at a small negative angle.

The domain dimensions are illustrated in Figure 1.5. At the inlet cartesian velocity components are speci…ed according to the angle of incidence. Freestream turbulence intensity is set at 0.05% which was the maximum value measured in the tunnel while the experiments were carried out [1]. At the outlet a zero static pressure gradient boundary condition was imposed.

The grids were generated in ICEM-HEXA. Three levels of re…nement were used and the grids are referred to as coarse, medium and …ne with 11920; 49625 and 202435 cells respectively. A grid convergence study is presented in Section 1.2.1. At each re…nement level the number of nodes along every block boundary was doubled. The medium grid is illustrated in Figure 6. In order to achieve a y^+ of approximately 1:0 the near wall spacing was set at 6:25 £ $10^{-5}c$. Particular care was taken to provide high quality cells around the leading edge and at the tip the cells have an aspect ratio of 1 : 1, the tip region is illustrated in the close-up view in Figure 1.6. Further down the chord very high aspect ratio cells are used in order to resolve the large ‡ow gradients normal to the wall and at the trailing edge the aspect ratio reduces to 1:10.

1.2 Results

The primary purpose of the validation study is to obtain an understanding of the ability of turbulence models to reproduce the leading edge separation bubbles of the type experienced in sail ‡ows. It is hoped that through this study it will be possible to determine what in‡uence the leading edge bubble has on the accuracy of sail simulations.

At 1 degree of incidence the leading edge bubble is of similar length to chord ratio to typical downwind

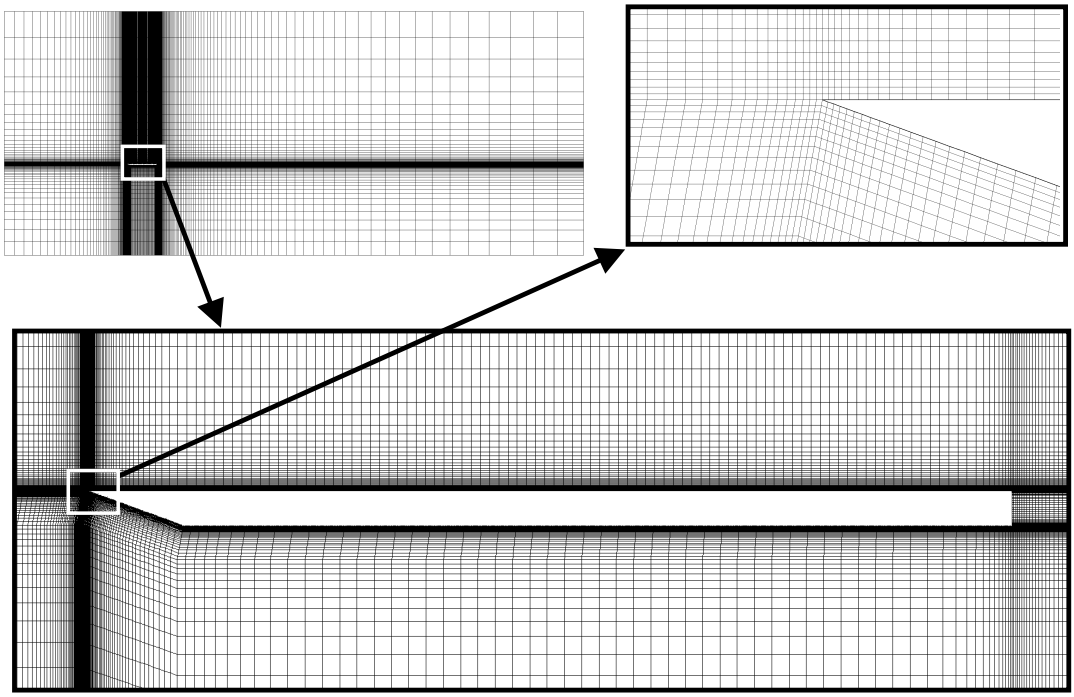

Figure 1.6: Computational grid for the ‡at plate (medium resolution).

sail ‡ows and the pressure distribution was more comparable to sail ‡ows than the other cases. Therefore, for the purpose of relevance, the validation study focuses on the case at 1 degree of incidence. At this angle the leading edge separation bubble stretches across the …rst 14% of the chord length (i.e. $X_R/c = 0{:}14$). Since the bubble is quite small fewer velocity measurements were taken within the bubble than the cases at higher angles. Consequently it was decided to also investigate the case of ® = 3 in order to gain a better understanding of the ‡ow within the separation bubble. At this higher angle of incidence the reattachment length, $X_R/c = 0{:}47$, i.e. the ‡ow is separated over almost half of the plate.

1.2.1 Grid convergence study

The grid convergence study was performed solely at ® = 3 and only with the SST turbulence model. Since ® = 3 involves a larger separated region than ® = 1 it is likely to be more prone to grid dependency. Therefore provided the grid independence is achieved for ® = 3, the same grid should be suitable for the ® = 1 case. Lift and drag coe¢cients are presented in Figure 1.7 for the sequence of grids. The force coe¢cients are plotted against $1/N[m]$ which is a measure of the grid spacing where N^2 is the total number of cells in the grid.

As the grid is re…ned there is a clear convergence of the lift and drag coe¢cients. The lift from the medium grid solution is within 0.015% of the …ne grid solution and drag is within 0.0055%, this indicates that the solutions are independent of the grid and subsequent re…nement is unlikely to result in any increased accuracy of the solution. Since forces are integrated properties there is a possibility that the grid convergence illustrated in Figure 1.7 could have occurred fortuitously. To con…rm that this is not the case the surface pressure distributions for the three grids are presented in Figure 1.8. Note that the spike in the pressure coe¢cient on the pressure side of the plate is caused by the shoulder at the end of

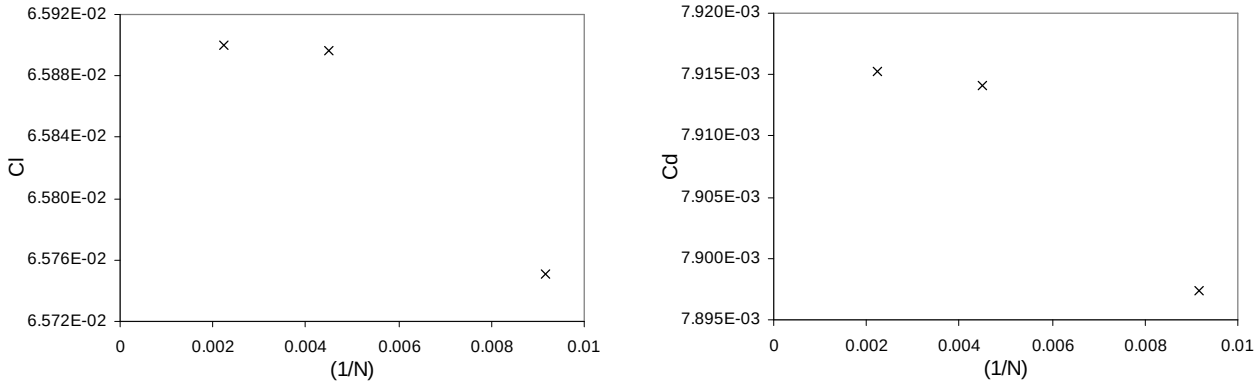

Figure 1.7: Grid convergence of the lift and drag coe¢cients.

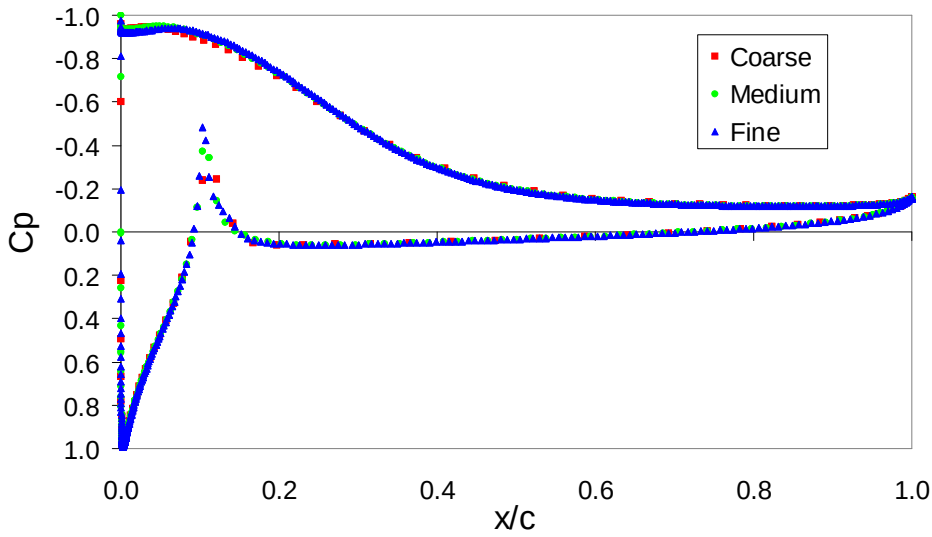

Figure 1.8: Grid convergence of the surface pressure coe¢cients (® = 3).

the chamfer.

The C_P curves for the medium and …ne grid lie almost directly upon one anther, the …ne grid solution has slightly less suction at the leading edge, however this e¤ect is minimal. Since the …ne grid and medium grid solutions are virtually identical the medium grid was chosen as the most suitable grid, and has been used for all subsequent simulations.

1.2.2 Comparison at ® = 1

Boundary layer pro…les in the leading edge bubble

Boundary layer velocity pro…les were measured by Crompton at 9 di¤erent chordwise locations along the plate using LDA. The measurement stations are located at x/c = f0:031; 0:125; 0:25; 0:375; 0:5; 0:625; 0:75; 0:875 As can be seen in Table 1.1 the reattachment lengths, X_R; computed using the SST and k ¡ $!$ models di¤er from the value determined by Crompton. The SST model overpredicts X_R by 5.8% and the k ¡ $!$ model overpredicts X_R by 24.0%.

	X_R
Crompton	0.14
SST	0.1486
k ¡ $!$	0.1841

Table 1.1: Reattachment lengths for the ‡at plate at ® = 1:

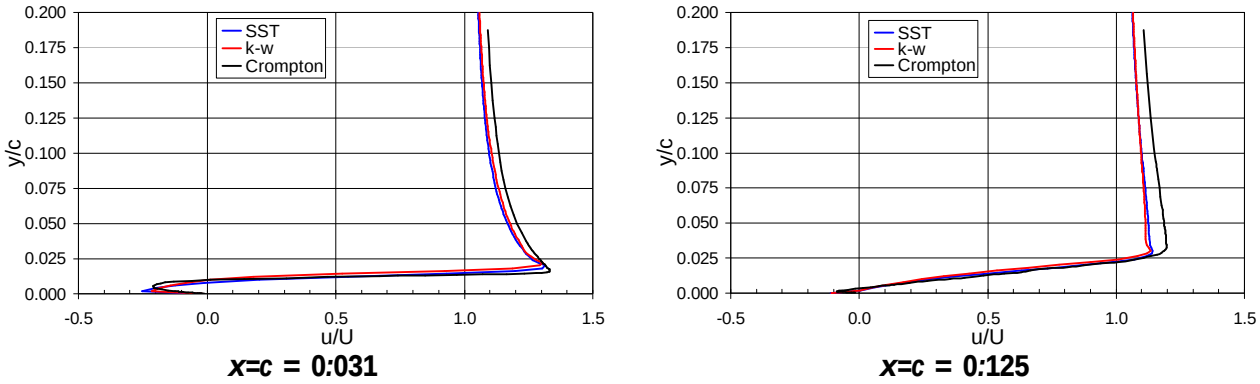

Figure 1.9: Chordwise velocity pro…les within the leading edge bubble (® = 1):

In order to make better comparison of the boundary layer pro…les the measurement stations are scaled by X_R so that for each model the station is in the same position relative to the reattachment point. For ® = 1 only the …rst two measurements stations are within the leading edge bubble, these pro…les are illustrated in Figure 1.9.

The portion of the ‡uid that is forced upstream at the reattachment point to form the recirculation region is accelerated by the favourable pressure gradient and forms a reversed boundary layer. Crompton reported a maximum reversed velocity of $0{:}4U_1$; whereas the CFD results predict much slower velocities with the SST model at $0{:}290U_1$ and the k ¡ $!$ model at $0{:}284U_1$: The reversed ‡ow velocities are much larger than usually experienced within separation bubbles, for example within short airfoil bubbles the reversed ‡ow is typically below $0{:}2U_1$ [1]: The reason for the high velocities in the ‡at plate case is the high entrainment rate in the shear layer which in turn provides energy to the reversed ‡ow through momentum balance. The CFD results predict a lower peak in the turbulent kinetic energy in the shear layer which is analogous to a lower entrainment rate. This is discussed further in Section 1.2.3 where the kinetic energy pro…les within the separation bubble are presented.

Boundary layer pro…les within the separation bubble are presented in greater detail in Figure 1.10. The reversed boundary layer is driven by a strong favourable pressure gradient which provides some degree of stablisation and the shape of the boundary layer pro…les in the experimental results indicate that relaminarisation is occuring. This e¤ect is illustrated in Figure 1.10, where the experimental results have very "laminar-like" pro…les. In comparison, the CFD results cannot emulate the relaminarisation process and conseqently predict much steeper near-wall velocity gradients.

One of the direct consequences of the more turbulent-like boundary layer pro…les predicted by the CFD results is their resistance to separation. In the CFD results the reversed boundary layer remains attached all the way to the leading edge and there is no secondary separation of the type reported by

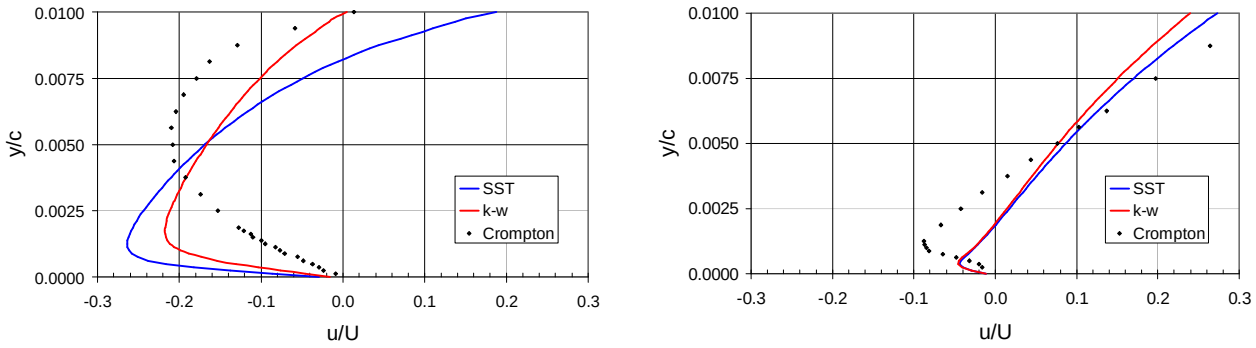

x/c = 0:031 x/c = 0:125

Figure 1.10: Near-wall chordwise velocity pro…les within the leading edge bubble (® = 1):

Crompton. Crompton suggests that the form of this bubble has signi…cant in‡uence on the development of the shear layer near the leading edge and consequently its in‡uence is likely to spread well downstream [1].

Boundary layer pro…les downstream of reattachment

A comparison of the boundary layer pro…les downstream of the reattachment point is presented in Figure 1.11. In general the CFD results compare well with the boundary layer pro…les measured by Crompton. From Figure 1.11 it is evident that the wind tunnel results give slightly fuller boundary layer results than the CFD however this e¤ect is di¢cult to quantify and it is hard to assess the structure of the di¤erent boundary layers.

In Figure 1.12 the boundary layer pro…les at x/c = 0:25 and 0:875 are presented using a log scale for the boundary layer height. Also plotted is a typical turbulent boundary layer at zero pressure gradient (ZPG) [7] as well as the log law of the wall (reference equation in introduction) and the viscous sublayer pro…le (reference equation in introduction).The pro…les in Figure 1.12 illustrate the recovery of the boundary layer. At x/c = 0:25 the experimental and CFD results have boundary layer pro…les that lie underneath both the log-law of the wall and the ZPG pro…le, i.e. the velocities in the sublayer and log-law regions are slower than would be expected for a typical turbulent boundary layer. This e¤ect is partially due to the slight adverse pressure gradient that the boundary layer must work against. However the low velocities in the log-law region must also be attributed to the reattachment process and in both the experimental and CFD results the boundary layer is in a recovery phase. At the reattachment point the normal u-velocity gradient ($@u/@y$) is zero at the wall (zero shear) and conseqently the near wall does not have the characteristic sharp increase of velocity known as the sublayer region. This near-wall behaviour in‡uences the entire velocity pro…le and at reattachment velocity pro…les have a more linear pro…le with signicifantly lower velocities than for a typical turbulent boundary layer. A boundary layer pro…le soon after reattachment is presented in Figure 1.13, the pro…le is approximately linear over the lower 75% of the boundary layer height (±). This pro…le is for the for the ® = 3 case at x/c = 0:5 which was the only angle of attack where a measurement staion was positioned soon after reattachment.

Also evident in the log pro…les of Figure 1.12 is that the near-wall velocities are much slower compared with typical turbulent boundary layer pro…les. This is a lag e¤ect from the reattachment process. As the boundary layer develops downstream it is the outer region that forms …rst and drives the development

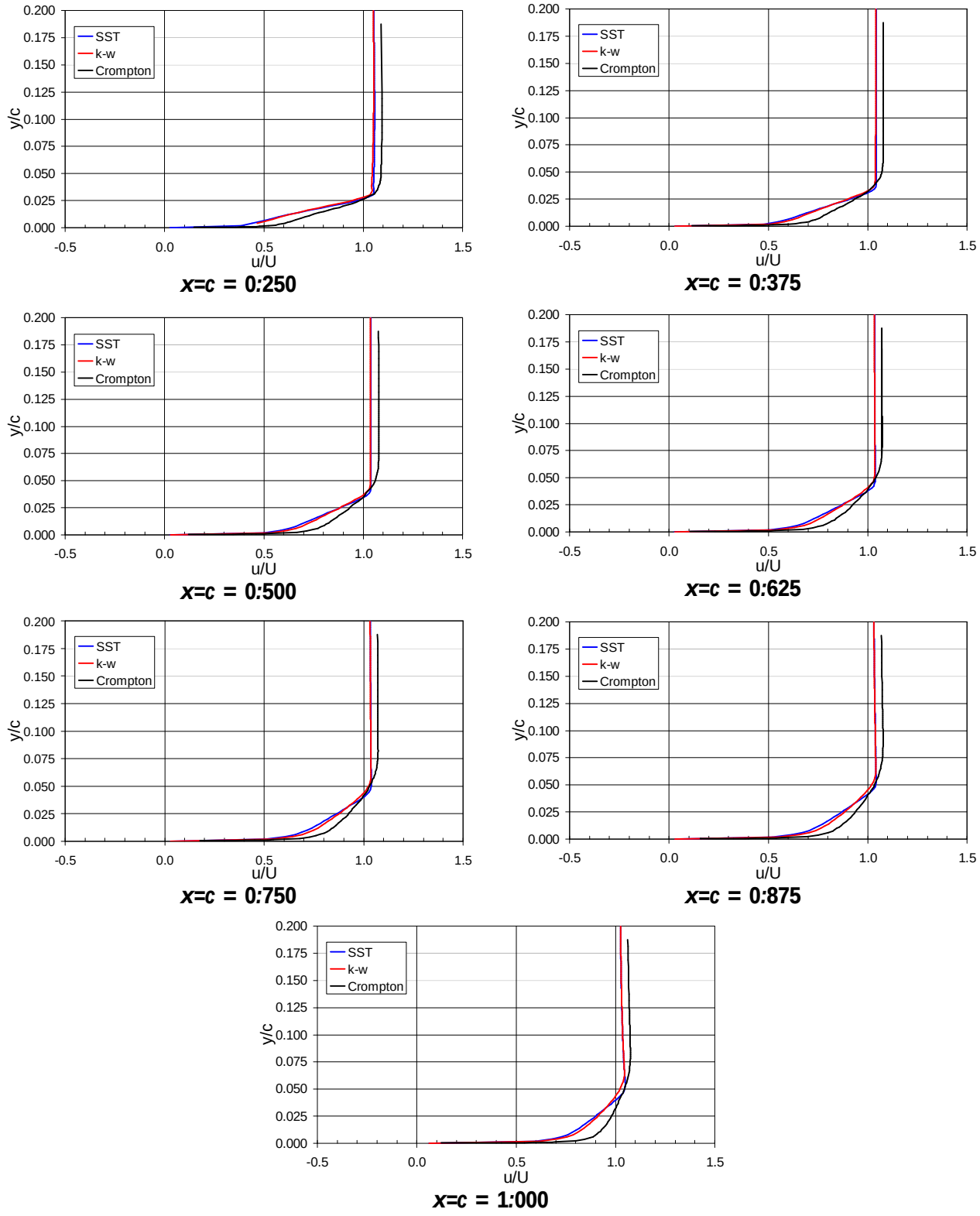

Figure 1.11: Chordwise velocity pro…les downstream of reattachment (® = 1):

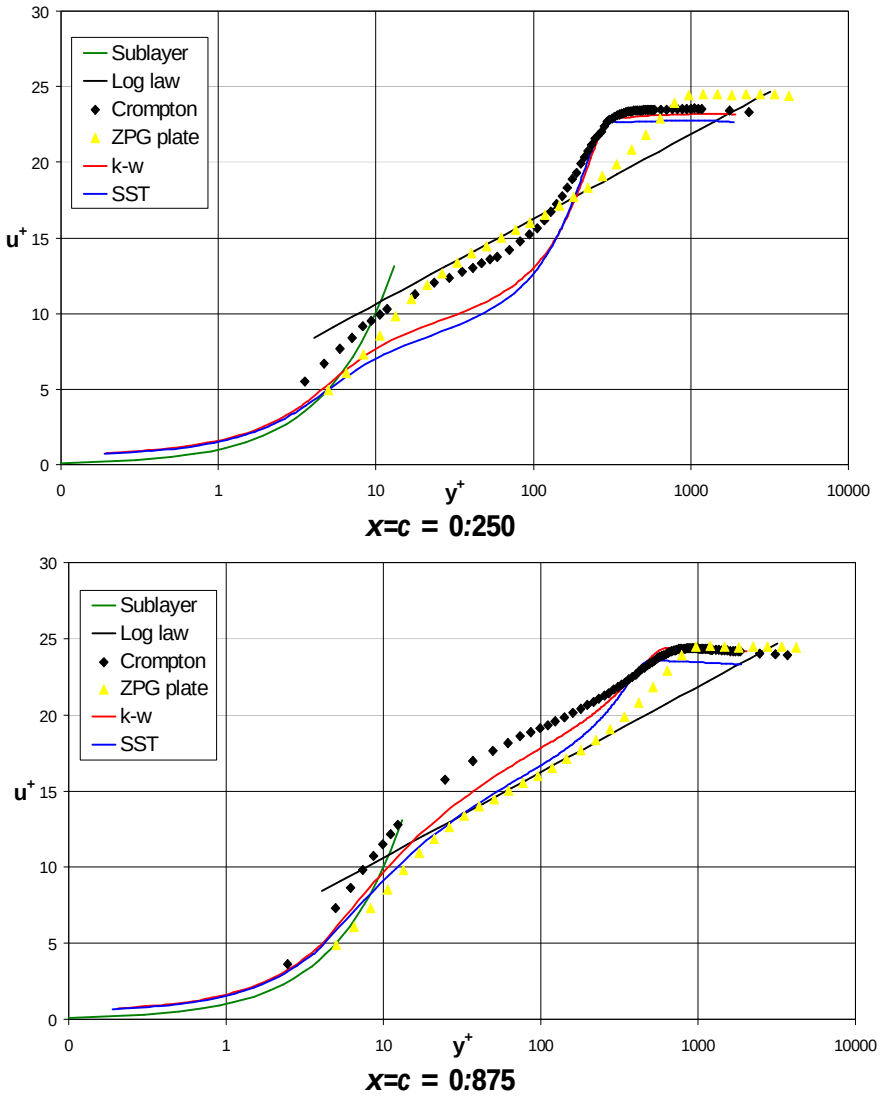

Figure 1.12: Chordwise velocity pro…les downstream of reattchment (log scale, ® = 1)*:*

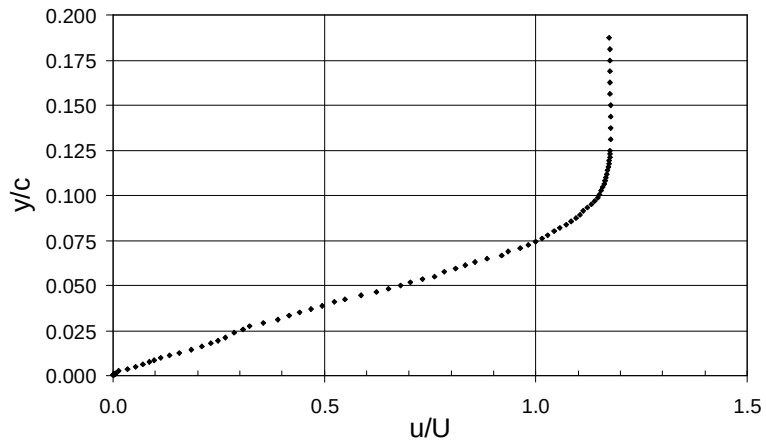

Figure 1.13: Boundary layer pro…le just after reattachment (Crompton) at ® = 3 and *x=c* = 0:5*:*

of the inner structure through the inwards entrainment of momentum. Unfortunately the experimental results do not have enough resolution to extend down throughout the viscous sublayer. However from the data that is available it appears that the sublayer in the experiments is has lower velocities than the CFD results. The CFD results overpredict the velocity magnitude near the wall and produce sublayer pro…les more typical of equillibrium boundary layer ‡ows. In the development of these turbulence models the model constants were calibrated to predict the correct asymptotic behaviour of both the ‡ow variables for simple homogenous boundary layers. Consequently when applied to ‡ows such as this, where the boundary layer structure is quite di¤erent to simple boundary layer ‡ows, they struggle to predict the correct near-wall behaviour.

Looking again at the results for $x=c$ = 0:25 (Figure 1.12) the pro…les predicted by the CFD also have lower velocities through the log-law region than the experimental results. This is a combination of the lower velocities that CFD predicts around reattachment and also because the CFD experiences slower recovery after reattachment.

At $x=c$ = 0:875 there is a slightly favourable pressure gradient and as expected the experimental results show an accelerated boundary layer (greater velocities than in the ZPG pro…le). It appears that through the log-region the boundary layer has recovered and is showing the typical response to the favourable pressure gradient. Within the viscous sublayer the velocities are still much lower than in the ZPG pro…le. In the log-law region the CFD results show slightly sluggish boundary layers despite the favourable pressure gradient, this would indicate that the in‡uence of reattachment point extends further downstream in the CFD than in the experiments. Slow post reattachment recovery of boundary layers is a common trait of turbulence models. So, Lai and Yoo [8] observed similar post-reattachment behaviour for the ‡ow past a backward facing step. For this case wall function based models were found to produce better results in the recovery region than Low Reynolds Number models. This is because wall functions, which are based on local-equilibrium arguments, force the ‡ow to asymtote to the log law-of-wall.

Figure 1.12 shows that the k ¡ $!$ model predicts pro…les that are slightly closer to the pro…les measured by Crompton than the SST model which seems to have a slower recovery from reattachment. However the di¤erences are small.

Pressure distributions

The pressure coe¢cient plot for the ‡at plate at ® = 1 is presented in Figure 1.14. In the experimental data the pressures continue to decrease downstream of the leading edge and has reached a minimum pressure at $x=c$ ' 0:045: Conversely the CFD results have a lower suction peak that is ‡atter and does not experience the gradual decrease in pressure over the forward half of the separation bubble that is seen in the experimental results. The leading edge radius is known to have an e¤ect on the local pressure coe¢cient with more rounded tips enabling the ‡ow to remain attached longer resulting in greater suction peaks. However Crompton paid special care to get a sharp leading edge and furthermore roundedness does not explain the di¤erences between the two turbulence models. The pressures within the leading bubble are related to the curvature of the shear layer (higher streamline curvature = lower pressure) and the experimental data has a shorter and fatter leading edge bubble which explains its higher suction peak. Additionally the secondary separation bubble that is present only in the experiments increases shear layer growth near the leading edge and hence contributes to the suction peak.

Another notable feature of Figure 1.14 is that between $x=c$ = 0:1 and $x=c$ = 0:2 the k ¡ $!$ model

predicts lower pressures than both the SST model and the experimental data. This is due to model overpredicting the length of the separation bubble. When the C_P curves are normalised with the reattachment length the comparison is good with the only signi…cant di¤erence being the large suction at the leading edge in the Crompton data.

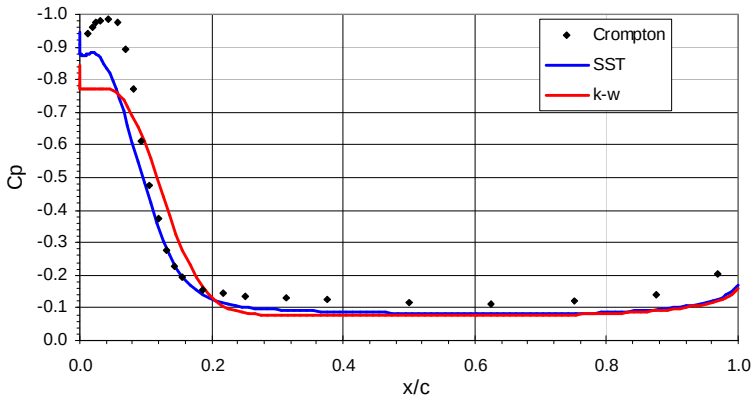

Figure 1.14: Pressure coe¢cient plot (® = 1).

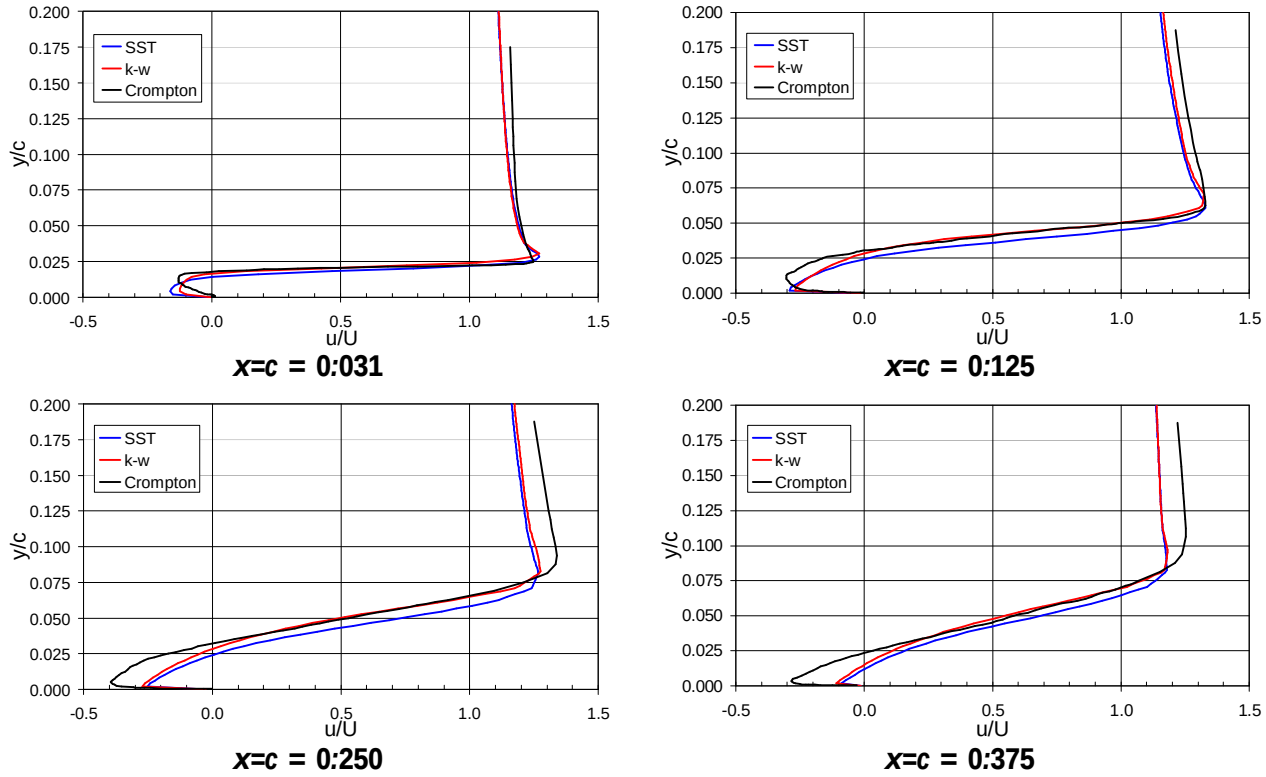

Figure 1.15: Chordwise velocity pro…les within the leading edge bubble(® = 3):

1.2.3 Comparison at ® = 3

Boundary layer pro…les in the leading edge bubble

The reattachment lengths for the ® = 3 case are presented in Table 1.2. The SST model underpredicts X_R by 6.4% and the k ¡ $!$ model overpredicts X_R by 8.4%. Once again the chordwise positioning of the pro…les presented in this chapter are scaled by X_R:

	X_R
Crompton	0.47
SST	0.4374
k ¡ $!$	0.5096

Table 1.2: Reattachment lengths for the ‡at plate at ® = 1:

Velocity Pro…les within the separation bubble are presented in Figure 1.15. Looking …rst at the measurement station closest to the reattachment point (x=c = 0:375); CFD predicts much lower reversed velocities than the experimental results. The measurement station at x=c = 0:25 coincides with approximately the mid length of the leading edge bubble, here the velocities are at their greatest, both at the outside edge of the shear layer and also in the reversed ‡ow region. In the reversed ‡ow region u = ¡0:393U_1 for the experimental results whereas the SST model predicts u = ¡0:252U_1 and the k ¡ $!$ model predicts u = ¡0:271U_1: At this measurement station the reversed boundary layer in the experiments is begining to show laminar-like features and is notably thicker than the CFD results. By x=c = 0:125 there is much less reversed ‡ow which is primarily due to mass ‡ow in the direction normal

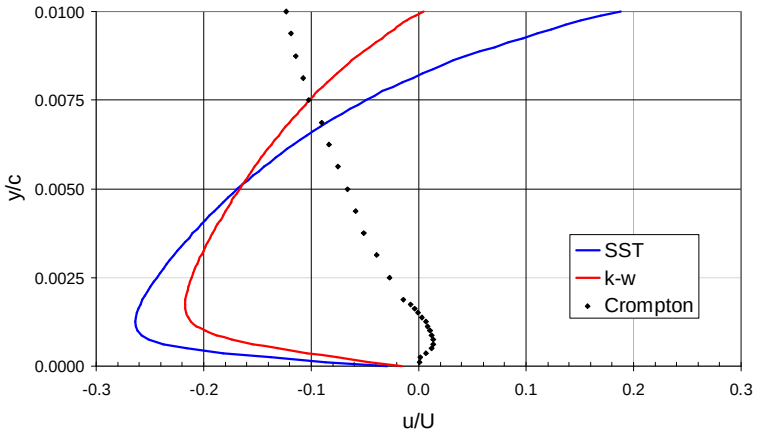

Figure 1.16: Near wall chordwise velocity pro…les at *x=c* = 0:031 (® = 3)*:*

to the plate but in the case of the experimental results the presence of an adverse pressure gradient also plays a role. At *x=c* = 0:031 the secondary separation bubble shows its presence in the experimental results close to the wall. The CFD results do not have this feature and the near wall ‡ow is reversed all the way to the leading edge. A close-up of the near wall region, showing the secondary bubble (in the experimental results), is presented in …gure 1.16.

Turbulent kinetic energy pro…les in the leading edge bubble

Further insight into the structure of the leading edge bubble can be gained from the pro…les of turbulent kinetic energy, *k;* that are presented in Figure 1.17. At *x=c* = 0:031 the experimental results show two peaks in the turbulent kinetic energy pro…le. The lower peak is associated with the secondary separation bubble that is not present in the CFD results. At the outer edge of the secondary separation bubble there is a region of high mean shear which increases production of turbulent kinetic energy. The second peak occurs at the point of in‡ection in the velocity pro…le in the outer shear layer which is also a region of high mean-shear. This second peak in kinetic energy is much stronger than the …rst as it is driven by the large velocities around the leading edge of the plate. This peak is much larger in the experimental results compared with the CFD, with the maximum turbulent kinetic energy 2.5 times greater than the SST model and 4.0 times greater than the *k* ¡ *!* model. It is believed that the large peak in *k* for the Crompton data is due to two e¤ects. Firstly the unstable shear layer ‡apping causes additional entrainment of kinetic energy and is a source of intermittency, and secondly the secondary recirculation bubble enhances the mean-shear in the leading edge region whichincreases the production of turbulent kinetic energy. Both of these e¤ects are not accounted for in the CFD results. The SST model predicts more turbulent kinetic energy in the shear layer than the *k* ¡ *!* model which is surprising since the SST relation is designed to limit the production of *k*. The SST model uses the *k* ¡ *!* model across the inner portion of the boundary layer out to the defect layer and the model blends to *k* ¡ ² by the outer edge of the boundary layer. Within the leading edge bubble the SST model blends to *k* ¡ ² across the inner region of the bubble and so it is the ²-equation that is solved across the shear layer. Therefore it appears that the ²-equation predicts a lower rate of dissipation of turbulent kinetic energy (*!* or ²=*k*) than the *!*-equation in the *k* ¡ *!* model (note that in the SST model the ²-equation is written in terms of *!*).

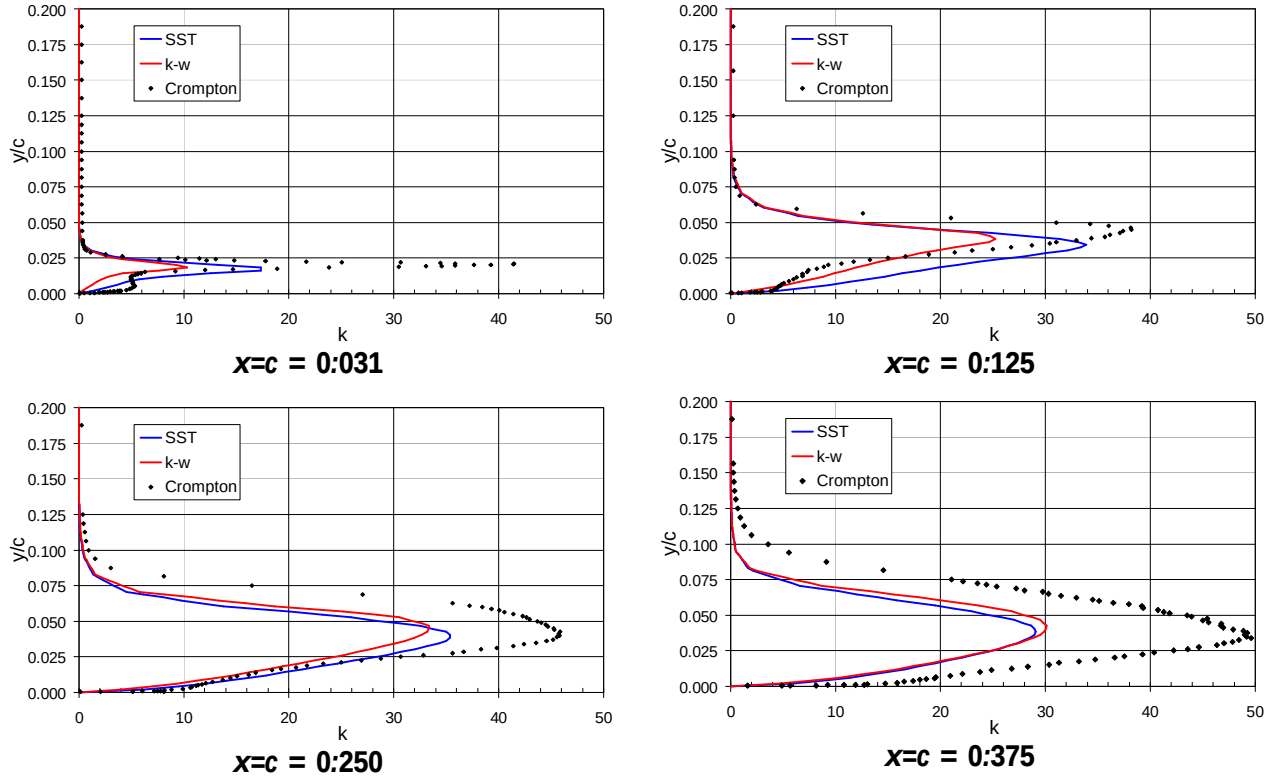

Figure 1.17: Chordwise velocity pro…les within the leading edge bubble(® = 3):

For the experimental results at *x=c* = 0:125 the magnitude of the turbulent kinetic energy in the shear layer is slightly lower than at the upstream station due to the diminished e¤ect of the secondary separation bubble which itself extends no further back than *x=c* = 0:045. The turbulent kinetic energy in the CFD results has increased for both the SST and *k* ¡ *!* model and the SST model is in better agreement with the experimental results. In both the CFD and the experimental results the peak in turbulent kinetc energy has widened due to the thickening of the shear layer. Near the all the experimental results have lower levels of turbulent kinetic energy than the CFD which is a result of the relamination process.

Between *x=c* = 0:125 and *x=c* = 0:25 the turbulent kinetic energy keeps a relatively constant pro…le for the SST model. Conversely the experimental results indicate that the kinetic energy in the shear layer is still increasing and the maximum entrainment rate has not yet been reached. The SST model predicts the shear layer to reach local equibrium prematurely, production of turbulent kinetic energy matches it's dissipation and the levels of *k* stop increasing. Between *x=c* = 0:250 and *x=c* = 0:375 both the SST and *k* ¡ *!* models predict a decrease in turbulent kinetic energy whereas in the experimental results *k* continues to increase. By this stage the *k* ¡ *!* model has also reached local equilibrium in the shear layer, whereas the experimental results indicate the turbulent kinetic energy in the shear layer is continuing to increase. The decrease in turbulent kinetic energy predicted by the CFD results is caused by the shear layer curving back towards the wall and the decelleration of the shear layer as it approaches reattachment. The experimetnal results show a similar drop in vertical velocity ‡uctuations (v^0) as the shear layer bends towards the wall, however this energy is converted to transverse (w^0) and streamwise (u^0) velocity ‡uctuations and thus the kinetic energy levels are retained.

At *x=c* = 0:375 both the SST model and the *k* ¡ *!* model predict peaks in turbulent kinetic energy

that are approximately 1.7 times smaller than in the experimental results. In the experimental results the kinetic energy peak is wider than the CFD indicating that the CFD results underpredict the shear layer thickness. This not surprising considering the entrainment rate is much greater in the experimental results.

In the CFD turbulent shear stress follows the same trends as the *k* pro…les, unfortunately turbulent shear stress data was not recorded int he experiments and so no comparison could be made.

Downstream of reattachment

The low turbulent kinetic energy across the rear half of the leading edge bubble in the CFD results has considerable e¤ects well downstream of reattachment and also within the leading edge bubble itself. As mentioned earlier the reversed boundary layer reaches much greater velocities in the experimental results. This is caused by greater entrainment which allows for higher shear layer curvature which leads to greater velocities. Similarily downstream of reattachment the boundary layers predicted by the CFD results are slower than in the experiments. This is partially a lag e¤ect from the lower velocities predicted by the CFD in the shear layer upstream of reattachment, but it is also apparent that the CFD results recover slowly from reattachment process. Downstream of the reattachment point the kinetic energy values are again lower in the experimental results which is a legacy e¤ect from the low values in the leading edge bubble. The higher levels of *k* in the experimental results enable much steeper gradients near the wall and conseqently the sublayer develops more rapidly enabling the boundary layer to regain a state of local equilibrium.

1.2.4 E¤ect of angle of attack

Look at plots of reattachment length with angle of attack and also the pressure coe¢cient plots. Also look at the pressure coe¤cient plots normalised to X_R.

1.2.5 Summary of Results

CFD vs Experiments

1. *The experiments experience greater growth and curvature of the shear layer which bounds the leading edge bubble.*

   REASON

   - Increased entrainment at the leading edge due to the secondary separation bubble and shear layer ‡apping.
   - Transport and production of turbulent kinetic energy dominates dissapation and hence *k* continues to increase along the length of the shear layer. CFD has di¢culities modelling non-equilibrium ‡ows due to the basic assumptions made in the derivation of the turbulence models.

   CONSEQUENCES

   - Reattachment is delayed in the CFD

- Lower suction peak in the CFD

2. *The reversed ‡ow in the leading edge bubble is subject to a favourable pressure gradient which causes relaminarisation. This e¤ect is not present in the CFD results.*

   REASON

   - The SST and k ¡ $!$ models are designed for fully turbulent ‡ows and are not capable of predicting relaminarisation.

   CONSEQUENCE

   - CFD fails to predict the secondary bubble at the leading edge.

3. *Downstream of reattachment the CFD pro…les recover towards turbulent equillibrium slowly compared with the experiments.*

   REASON

   - The developing boundary layer is dominated by two distinctly di¤erent spectrums of eddy scales; the scales in the outer region of the near wall that have their origin in the separated shear layer, and the scales in the inner region associated with the development of the new boundary layer.

   CONSEQUENCES

   - Velocities in the CFD boundary layer pro…les are slower than in the experiments and are therefore more subseptable to separation
   - Higher pressure coe¢cients in the CFD results.

SST vs k ¡ $!$

1. The SST model captures the leading edge bubble more accurately than k ¡ $!$; it predicts a reattachment length that is closer to the experimental value and does a better job of predicting the pressure coe¢cient in the vicinity of the leading edge bubble.

   REASON

   - The SST model predicts greater turbulent kinetic energy near the leading edge and therefore predicts greater shear layer growth. As a results the shear layer has more curcature and bends back towards the plate earlier than the k ¡ $!$ model.

2. Downstream of reattachment the k ¡ $!$ model predicts a more rapid boundary layer recovery than the SST model, however the recovery is still slower than the experimental results.

   REASON

[2] **Since there are two distinctly di¤erent length scales interacting in the recovery region a two-equation model, that operates using just one length scale ($k^{1=2}=!$); cannot be expected to perform well. The di¤ence between the velocity pro…les are small and are likely to be a result of the SST model blending to the ²-equation through the outer region of the boundary layer.**

1.3 Comparison with other ‡ow …elds

General dissucusion of the signi…cance of this test case with reference to ‡ows that posess similar traits. Esp Sail ‡ows. Disscussion about similar test cases e.g. backward facing step.

1.4 Conclusions

Bibliography

[1] M. J. Crompton, *The Thin Aerofoil Leading Edge Bubble*, PhD thesis, University of Bristol, 2001.

[2] B. G. Newman and M.-C. Tse, Incompressible Flow Past a Flat Plate Aerofoil with Leading Edge Separation Bubble, Aeronautical Journal 96, 57–64 (1992).

[3] D. M. Driver, H. L. Seegmiller, and J. G. Marvin, Time-Dependent Behavior of a Reattaching Shear Layer, AIAA Journal 25(7), 914–919 (1987).

[4] L. F. Crabtree, The Formation of Regions of Separated Flow on Wing Surfaces, Technical Report R&M-3122, Aeronautical Research Council, London, 1957.

[5] D. C. Wilcox, *Turbulence Modeling for CFD*, Gri¢n Printing, California, 2nd edition edition, 1998.

[6] D. C. Wilcox, Simulation of Transition with a Two-Equation Model, AIAA Journal 32(2), 247–255 (1994).

[7] J. Österlund, *Experimental Studies of Zero Pressure-Gradient Turbulent Boundary Layer Flow*, PhD thesis, Kungl Tekniska Högskolan, 1999.

[8] R. M. C. So and Y. G. Lai, Low-Reynolds-Number Modeling of Flows over a Backward Facing Step, Journal of Applied Mathematics and Physics 39, 13–27 (1988).